BioNanoSci. (2011) 1:63–77
DOI 10.1007/s12668-011-0014-5

Surface Nanoengineering Inspired by Evolution

Thor Christian Hobæk · Kristian Greger Leinan · Hans Petter Leinaas · Christian Thaulow

Published online: 2 August 2011

Abstract Through evolution, nature has optimised structures and materials with a hierarchy from the macro- to the nanoscale. Biological materials are very sophisticated in the way they solve challenges associated with life. Some properties of commercial interest found in nature are self-cleaning, aerodynamic lift, anti-adhesion, water harvesting, water-floating and staying dry. Biomimetics, to learn from nature, has been used for centuries to create new innovative devices. With the use of "nanotools", it is possible to design hierarchical surface structures with exceptional functional properties. In this paper, an overview of interesting surface properties with biomimetic potential, strategies for nano-manipulation of surfaces, potential industrial applications and the potential of using atomistic modelling to optimise surface structuring are discussed.

Keywords Biomimetics · Bioinspired · Nanotechnology · Surfaces · Superhydrophobicity · Atomistic modelling

1 Introduction

For centuries, human beings have been fascinated and inspired by nature's design and mechanisms. Leonardo da Vinci examined the flight behaviour of birds and proposed mechanisms for flight by machines in his Codex on the Flight of Birds from 1505. At the beginning of the twentieth century, the Wright brothers used the observation that birds glide and do not flap their wings repeatedly as an inspiration for building the world's first successful airplane. Later, wing design and geometry has inspired the construction of modern aircrafts. The U2 spy plane was developed for the US Air Force in the 1950s with the wings having a high aspect ratio, that is the length-to-width ratio, to achieve a long flight endurance similar to the great albatross (Diomedea). Oppositely, the British-designed Harrier Jump Jet have a small aspect ratio, similar to the pheasant (Phasianidae), which gives a high lift force and enables it to take off and land vertically. The classical work by D'Arcy W. Thompson describing biological systems as structures contains many more examples [1].

Nature has gone through evolution during the 3.8 billion years that life has existed on earth [2]. Through this period, only the most successful and optimised designs have survived. Biological materials are produced by self-assembly of only a few elements into complex hierarchical structures, ranging from the macroscale to the atomic scale, in a way that costs minimal energy, resulting in a great diversity of functional properties [3, 4]. Nature is also dynamic; it responds rapidly to environmental changes and has the ability to self-repair minor damage [5]. It has to use whatever material available locally, typically exceptional brittle minerals, or rely on weak H-bonding in spider silk, or Van der Waals forces in the gecko's foot [6]. For instance, shells of molluscs consist of approximately 95 wt.% $CaCO_3$. Through the way the material is organised, embedded in a protein network, the fracture toughness of a natural shell is 3,000 times that of pure monolithic $CaCO_3$ [7]. The surface energy, which will be described later, plays an important role in the initiation and propagation of fracture, as this process involves introducing new interfaces in the

T. C. Hobæk · K. G. Leinan · C. Thaulow (✉)
Department of Engineering Design and Materials,
Norwegian University of Science and Technology,
Trondheim NO-7491, Norway
e-mail: christian.thaulow@ntnu.no

H. P. Leinaas
Department of Biology, University of Oslo,
Oslo NO-0316, Norway

material. Hence, there exist an interesting link between nanoscale surface structuring and fracture resistance.

Biomimetic is a term consisting of the Greek words bios and mimesis, translated to life and imitation in English, respectively. The American inventor Otto Schmitt first coined the term in 1957 to describe a physical device that mimicked the electrical action of a nerve. The term has since then been used to describe the imitation of mechanisms and structures found in nature to establish new technology. The term bio-inspired is however a more broad definition, as using nature as a source of inspiration might solve other problems than what is encountered by living systems. Thus, simply copying nature should not be sole strategy for engineers and scientists.

The field of biomimetics is highly interdisciplinary, with elements from biology, physics, chemistry and materials science. With the advancement of nanotechnology, scientists are able to study structural details smaller than ever before. As will be discussed later in this review, nanoscale surface texture has a profound effect on the observable macroscopic phenomenon in nature. Through surface nano-engineering, that is producing surface structures using micro- and nanofabrication techniques, it is possible to mimic those to produce new functional materials. Together with the great selection of engineering materials available, we can potentially go nature one better.

The purpose of this review is to provide an overview of biomimetics of various functional surfaces. A short overview of relevant wetting theory is given, such as explaining superhydrophobicity and the effect surface texture has on the wetting properties. This section is followed by a description of biological surface mechanisms such as the water capturing of the Namib Desert Beetle, the floating ability of the water strider, the ability to stay dry while submerged under water by the water fern and the self-cleaning effect exhibited by the lotus leaf. The connection between surface nanostructures and functional properties will be emphasised. Potential commercial applications of functional materials inspired by the presented biological examples will be outlined. Finally, the potential of using atomistic modelling as a computational tool to optimise surface structuring is discussed.

2 Theoretical Concepts

Wetting describes how water spreads out on a solid surface, a result of intermolecular forces. Characteristic of the wetting behaviour is the contact angle at the triple point, which is defined as the position where the three phases of solid, liquid and gas meet. Contact angle is defined in terms of the surface tension or surface energy; two equivalent terms which describes the force per unit length (N/m) and the work done per unit area (J/m^2) to create an interface [8]. Equilibrium is predicted by the Young-Dupré equation, which is a balance of the surface tension acting on the triple line

$$\cos\theta_0 = \frac{\gamma_{SG} - \gamma_{SL}}{\gamma_{LG}} \tag{1}$$

This relation provides a useful model to predict the wetting behaviour based on surface tensions, which are constants characteristic for different liquids and solids. The surface tension of water against air at 25°C is 72 mN/m [9]. Surfaces with low surface energy are often hydrophobic in contact with water, resulting in high contact angles.

The relation above is based on the assumption that the surface is flat. When surface roughness is taken into account, different wetting behaviour is observed (see Fig. 1). This is well described by the Wenzel [10] and Cassie–Baxter [11] equations given as

$$\cos\theta = r\cos\theta_0 \tag{2}$$

$$\cos\theta = (1 + r_f\cos\theta_0)f_{SL} - 1 \tag{3}$$

respectively, where θ_0 is the smooth contact angle, r is a roughness factor greater than 1, r_f is the roughness factor of the wetted area and f_{SL} is the fractional area of the wetted solid. Notice that when $f_{SL}=1$, the solid is completely wetted, $r_f=r$ and the Cassie–Baxter state is reduced to the Wenzel state.

Depending on the surface texture, either of the two states represents a global energy minima [12, 13]. Transition between the two wetting phases can occur by external factors such as vibrations [14]. A thorough derivation of Eqs. 1, 2 and 3 can be found in the work by Whyman et al. [15].

The Cassie–Baxter wetting state occurs for several of the biological surfaces discussed in this paper. In this state, water droplets rest on the uneven surface with air trapped in the local valleys, similar to a fakir resting on a bed of nails. Such kind of surfaces are often superhydrophobic, that is if the contact angle is above 150° [16].

In contrast, superhydrophilic surfaces have a contact angle below 10°. Superhydrophobic or syperhydrophilic surfaces can be achieved by increasing the roughness. Increasing the roughness factor in Eq. 2 for the Wenzel wetting state, increases the contact angle if $\theta_0 > 90°$ (hydrophobic). However, if $\theta_0 < 90°$ (hydrophilic) increasing roughness will make the surface more hydrophilic, illustrated in Fig. 2. The transition between superhydrophobicity and syperhydrophilicity can be very sharp for contact angles around 90° and extreme surface roughness, so that it can be induced by small changes in surface energy, for instance through heating [17].

When describing wetting behaviour, it is also important to take the kinetic wetting behaviour into account. A high contact angle does not always mean that the surface is water repellent [18]. This can be described by the contact angle hysteresis,

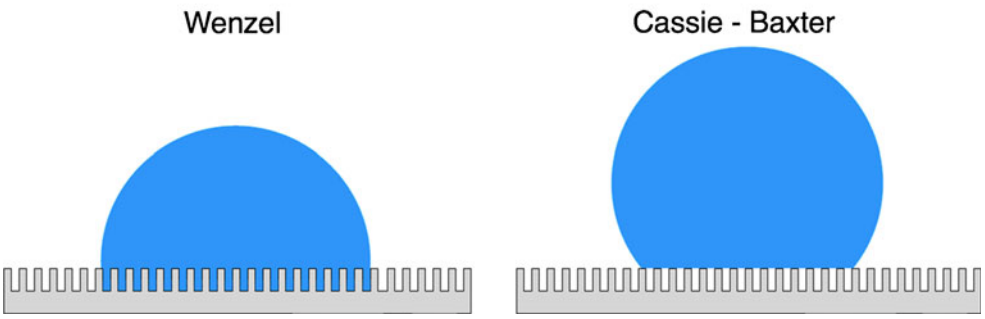

Fig. 1 The droplet in the Wenzel state wets the rough surface, while it rests on top of the pillars in the non-wetting Cassie Baxter state, with pockets of air trapped beneath

defined as the difference between the advancing and receding angle, and the sliding angle where the droplet start to roll off the surface [19]. The kinetics of wetting is much less understood than for droplets in equilibrium, so most of the current theoretical research is focusing on this area [18, 20, 21]. It is believed that a low contact hysteresis is a requirement of a stable Cassie–Baxter wetting state [22].

So far, the scale of roughness has not been discussed. Imagine a surface of square pillars illustrated in Fig. 3. The area fraction f in the Cassie–Baxter state is independent on the roughness scale. However, the triple line length L_T, which is the length of the total perimeter of the three different phases increase dramatically with decreasing roughness scale. Zheng et al. [23] defined a scale of roughness parameter S, equal to

$$S = \frac{A}{L} = \frac{a^2}{4a} = \frac{a}{4} \tag{4}$$

where, A is the top surface area of the pillars and L is the boundary length. The total triple line length L_T can then be defined as

$$L_T = \frac{f}{S} \tag{5}$$

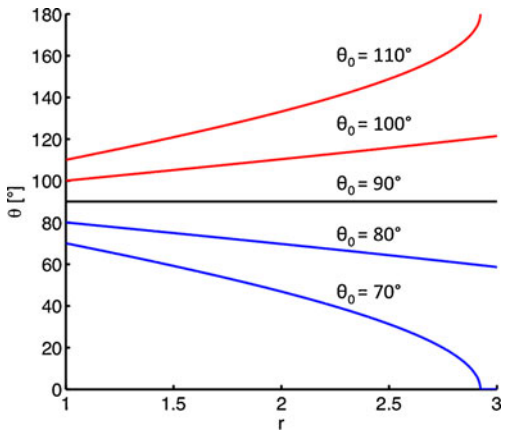

Fig. 2 The effect of increasing the roughness factor r on surfaces with different inherent contact angles described by the Wenzel equation. Inherently hydrophobic surfaces (*red curve*) becomes more hydrophobic by increasing the contact angle, while inherently hydrophilic surfaces (*blue curve*) becomes more hydrophilic

For a surface covered with square pillars with $a = b = 1$ mm, the scale of roughness is equal to $S = 0.25$ mm and the area fraction $f = 0.25$. Thus, for a 1 m^2 surface, $L_T = 1$ km. However, if the pillar side length is reduced by a 1,000-fold to $a = b = 1$ μm, the area fraction f will be constant, but now the total triple line length has increased to 1,000 km. Increasing the triple line length is associated by an increasing cost in terms of energy [24]. Thus, one should indeed expect the contact angle to increase with increasing triple line length. This was confirmed by Zheng et al. who measured contact angles for several microfabricated pillars with different scale of roughness [23], see Fig. 4. A modified version of the Cassie-Baxter equation were fitted to the experimental data, taking the scale of roughness into account

$$\cos\theta = \left((1 + \cos\theta_0)\left(1 - \frac{l_{cr}}{S}\right)\right) f - 1 \tag{6}$$

where, l_{cr} is an intrinsic fitting parameter depending on the surface chemistry of the material. The results suggest that nanoscale surface roughness is necessary in order to achieve superhydrophobicity.

3 Examples

3.1 Biological Surfaces

The following section gives an overview of some of the functional surfaces found in biology, which all have properties of commercial interest.

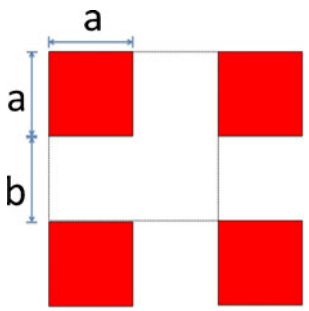

Fig. 3 Model surface with squared pillars. In the Cassie–Baxter state, for simplicity, only the top area of the pillars is wetted. The area fraction f can thus be defined by the two parameters a and b

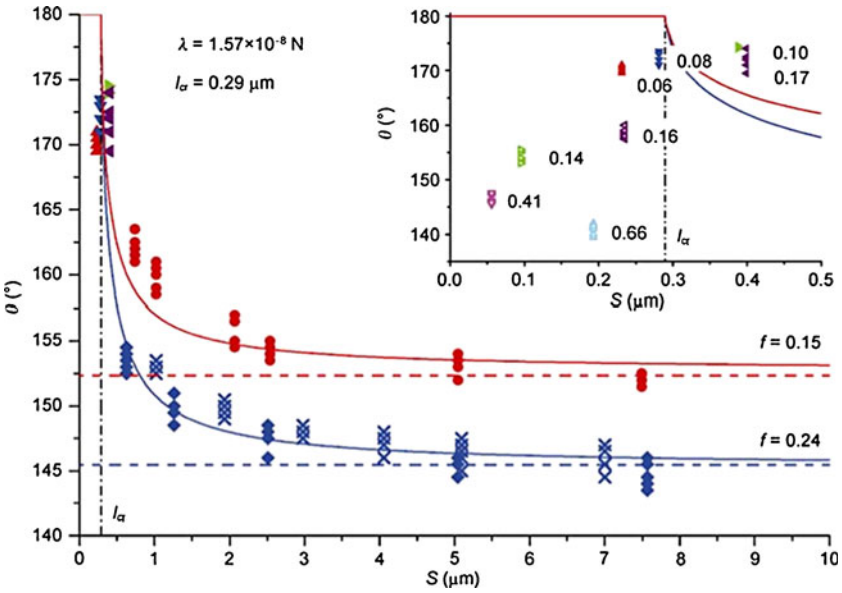

Fig. 4 The measured contact angles as a function of size of fabricated micropillars. The *red* and *blue curves* represent different filling factors according to the Cassie–Baxter equation (*dashed lines*). Decreasing the scale of roughness and keeping the area fraction constant, results in higher contact angles, reaching a critical value l_{cr} with a length of approximately 0.29 μm. With kind permission from Springer Science+Business Media: Science China Physics, Mechanics & Astronomy, Small is beautiful, and dry, 53, 2010, 535–549, QuanShui Zheng, Fig. 2

3.1.1 Water Collection

Creatures living in arid areas are challenged by the shortage of water. This problem is overcome by the Namib Desert Beetle (*Stenocara gracilipes*), which collects water during the morning when the humidity in the air is high [25]. The size of the fog droplets is small, 1–40 μm in diameter, so they are easily carried away by the wind. To collect water, the beetle brings its back to a tilt by raising its hind legs so that the humid air impacts the beetle's back. The surface structure of the beetle's back is bumpy, consisting of alternating wax-coated, hydrophobic areas and hydrophilic non-waxy regions at the peak of the bumps (see Fig. 5d). The bumps are about 500 μm in diameter, separated by a distance of 500–1,500 μm. The hydrophilic regions have a smooth surface, whereas the hydrophobic regions have protuberances shaped as hemispheres with 10 μm in diameter, placed in an hexagonal array [25].

The hydrophilic regions act as seeding points where the water vapour condenses. During this process, droplets that are formed increase in size over time. Eventually, the droplets reach a critical size when the capillary forces attaching the droplet to the surface, is overcome by the sum of gravity and the force experienced by the wind. They then detach and starts rolling over the hydrophobic areas towards the beetle's mouth, where it is consumed.

3.1.2 Water Floating

Some insects like the water strider have the ability to stay floating and walk efficiently on top of water. Even when large raindrops disturb the water nearby, it simply bounces away and remains floating. Due to the hierarchical structures and the surface chemistry of the water strider legs, the water resistance is extremely high (see Fig. 5a–c) [26, 27]. The legs are covered by a large number of oriented tiny hairs called micro-setae, which are inclined by an angle of 20° with the leg surface and with a diameter ranging from typically hundreds of nanometres to about 3 μm and a length of about 50 μm. Each micro-setae are further covered by fine nano-sized grooves on the surface, which traps pockets of air underneath the water surface, characteristic of the Cassie–Baxter wetting state. The legs are able to support a weight of about 15 times the total body weight of the insect before the water interface collapse. At that point, the volume of displaced water is about 300 times that of the leg itself.

Figure 6 shows a schematic of the water repellent effect of the water strider leg by Feng et al. [27]. Based on measuring the depth of the dimple that the leg is able to create when pushed down into the water, the contact angle of the legs were estimated to be around 168°. The contact angle θ_w on the secreted waxes on the legs' surface is however only 105°. This is not sufficient to explain the observed superhydrophobicity. By using the Cassie–Baxter model (Eq. 3), it is possible to predict the contact angle of the oriented micro-setae on the leg's surface θ_s, by using the measured area fraction $f = \frac{d}{S}$, which is in the range of 0.05–0.1, as

$$\cos\theta_1 = (\pi - \theta_s) f \cos\theta_s - (1 - f \sin\theta_s) \quad (7)$$

To achieve a contact angle of θ_1=168°, the seta must have a contact angle θ_s of at least 125°, which is larger than θ_w. In other words, the micro-setae structure is not enough to yield superhydrophobicity. However, by applying the Cassie–Baxter model to the nanoscale grooves on the

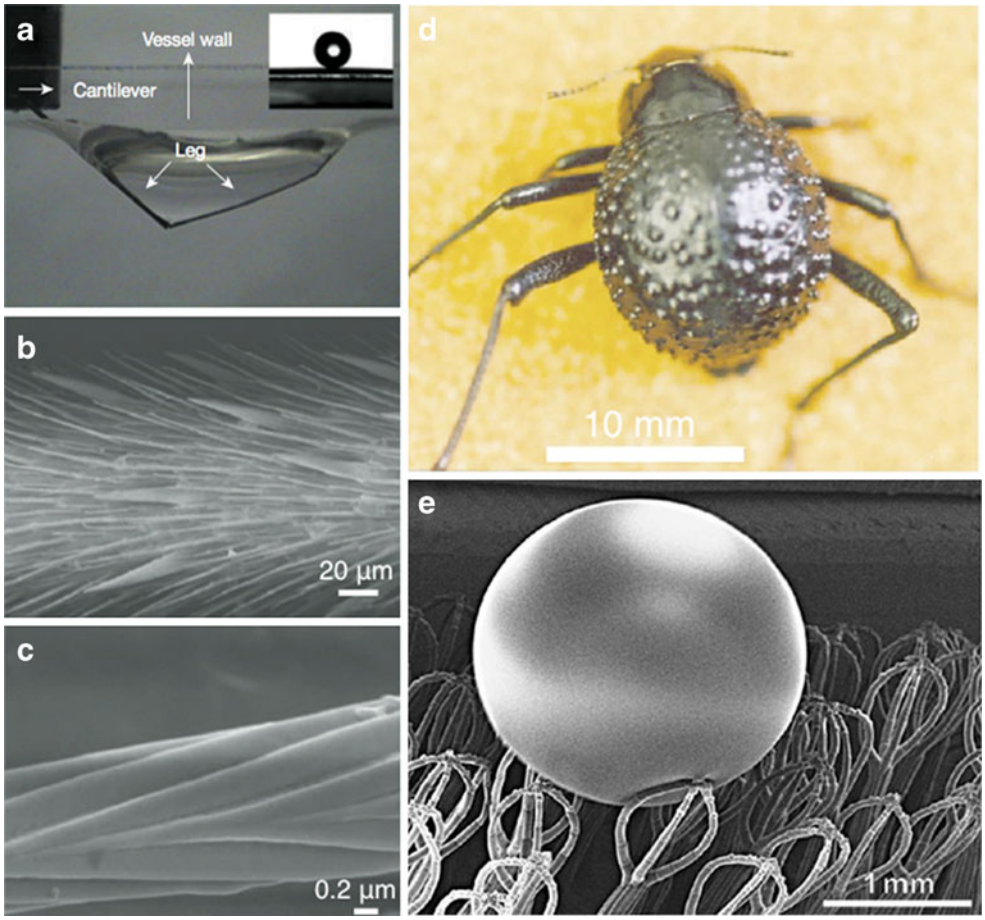

Fig. 5 **a** The water repellent leg of the water strider displaces water when it is pressed against the water surface. **b** The legs are covered by ordered microsetae. **c** Single microsetae have fine nanoscale grooved structures, responsible for trapping of small air bubbles, adapted with permission from Macmillan Publishers Ltd: Nature [26], copyright 2004. **d** The Namib Desert Beetle has hydrophilic bumps superimposed on its superhydrophobic back. The hydrophilic regions capture water from the morning fog, which eventually rolls off into the beetle's mouth, adapted with permission from Macmillan Publishers Ltd: Nature [25], copyright 2001. **e** Low-temperature SEM of a frozen leaf of the water fern, with applied droplet of a water–glycerol solution. Hydrophobic nanoscale waxes cover the multicellular hairs on the surface, except at the patched ends. The superhydrophobicity of the hairs prevents wetting of the leaf surface, while the hydrophilic ends stabilises the water–air interface when the leaf is submerged. W. Barthlott, The *Salvinia* paradox: superhydrophobic surfaces with hydrophilic pins for air retention under water, Advanced Materials, 2010, 22, 2325–2328, Copyright Wiley-VCH Verlag GmbH & Co. KGaA. Reproduced with permission

micro-setae surface, with $f' = \frac{2d'}{S'} \approx \frac{2}{3}$, the contact angle of the seta,

$$\cos\theta_s = (\pi - \theta_w)f' \cos\theta_w - (1 - f' \cos\theta_w) \quad (8)$$

is around 125°, which corresponds well with the measured dimple height. Thus, it is the hierarchical surface structure of the water strider leg that is responsible for its water-floating ability.

The water fern plant Salvinia exhibits a similar strategy. While submerged under water, the leaf surface shows a silvery reflection, resulting from trapped air bubbles. The water fern is able to retain an air film under water for 17 days [28]. The hierarchical surface of the Salvinia consists of multicellular hair structures covered by hydrophobic waxes at the nanoscale. The hairs branch into four smaller multicellular hairs at the end, which eventually merge together and form a flat patch at the very end [29]. While most of the hairs are covered with waxes, making them superhydrophobic, the patch ends display a smooth, hydrophilic surface with no wax crystals superimposed.

Droplets form a nearly spherical shape, resting on top of the hairy structures (see Fig. 5e). The water sticks to the hydrophilic patches, while the water–air interface is prevented from penetrating the space between the hairs due to the superhydrophobic waxes. The pinning of water at the patches stabilises the water–air interface during pressure fluctuations caused by turbulent flow. To retain the air film at the surface, the energy required for water to penetrate between the hairs have to be maximised. On the other hand, because the water is highly pinned to the hydrophilic ends, energy is required to remove the interface far away from the surface. The combined

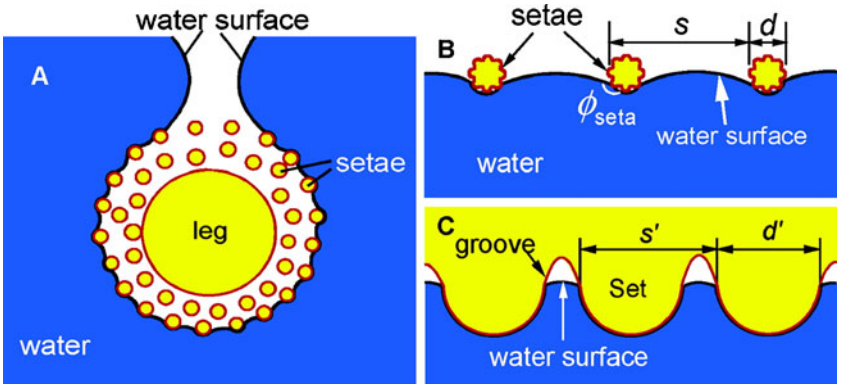

Fig. 6 Schematics of the water strider leg structure and the liquid–air interface. **a** A cross-section of one leg with superimposed tiny hairs, called setae. Because of the weight of the water strider, the water surface is displaced (see also Fig. 5a), but the legs are not wetted. **b** Only the setae are believed to be in contact with water. The area fraction of the liquid *f*, which is in contact with the setae, can be defined by the setae diameter divided by the separation length of individual hairs. **c** The setae are not completely wetted, as the nanoscale grooves have trapped pockets of air. Here, the area fraction *f'* is given by the radius of curvature of the grooves, and the separation between individual grooves. Reprinted with permission from Xi-Qiao Feng, Superior water repellency of water strider legs with hierarchical structures: experiments and analysis, Langmuir, 2007, 23, 4892–4896. Copyright 2007 American Chemical Society

effect of this structural arrangement is therefore to keep the leaf surface dry.

3.1.3 Self-Cleaning and Anti-Adhesion

Some plants growing in wet environments such as marshland exhibits self-cleaning and anti-adhesive functions. One of them is the Lotus flower (*Nelumbo nucifera*), which has been a symbol of purity in Asian traditions for at least 2,000 years [30]. Even when emerging from muddy waters, it stays unaffected by pollution. It is said to be self-cleaning, demonstrated by Barthlott et al. [31]. The phenomenon is often referred to as the "Lotus Effect". The surface structure along with the chemical properties of the cuticle is responsible for this effect. This results in a contact angle of 162° [32] and a contact angle hysteresis of about 4° [33]. The self-cleaning of the lotus leaf is independent of the chemical composition of adhered particles and it functions as a defence mechanism against potentially dangerous plant pathogens like bacteria and fungi. Also, keeping the surface dry is important especially in humid environments, as diffusion of CO_2 necessary for the photosynthesis is 10,000 times slower through water than air [34].

The surface roughness at two hierarchical scales together with the surface chemistry leads to a superhydrophobic surface with a very high contact angle, a characteristic that is also present on many other types of leaves [32, 35]. The surface structure consists of convex papilla shaped cells with a superimposed layer of three-dimensional crystal waxes (see Fig. 7). The papillose cells are randomly distributed across the surface of the leaf, with variations in height and distance separating individual cells. Characteristic of the wax crystals are that they form hollow structures, called tubules. They contain a high amount of nonacosan-10-ol, which is a secondary alcohol with a low surface energy. The tubules are typically 0.3–1.1 μm in length and 0.1–0.2 μm in diameter [30].

Because of the hierarchical surface structure of the lotus leaf, air becomes trapped in the cavities between the convex cells, leading to a Cassie–Baxter wetting state [36–38]. Superhydrophobicity can however be achieved solely by one-scale roughness on the nano-scale [38]. The role of the dual-scale surface roughness is partially to enhance the pressure stability of the water–air interface resting on the wax crystals [39]. Also, hierarchical surfaces have a higher resistance against mechanical wear compared to a surface with only nanoscale roughness, as a smaller fraction of the surface area is available for wear damage [32].

When water droplets hit the leaf surface, dust particles are washed away [31]. Due to the low surface energy and the extreme surface roughness, the adhesive force between pollutant particles and the surface is very small. Only weak van der Waals forces bind the particle to the surface [40]. Because the capillary forces of water overcome the adhesive force, the lotus leaf is practically self-cleaning.

3.1.4 Pigeon Feathers

Feathers are important for birds' ability to fly. They reduce drag by reducing vortices, repel water to keep the bird light enough to fly, keep the birds warm and give colour. Bormashenko et al. studied the hydrophobic effect of pigeon feathers and found that the Cassie–Baxter wetting regime describes the feather surface well [41]. The network of barbs and barbules supports the water and leaves pockets of air between the substrate and the drop (see Fig. 6). This is attributed to the double-scale roughness of the feather suit.

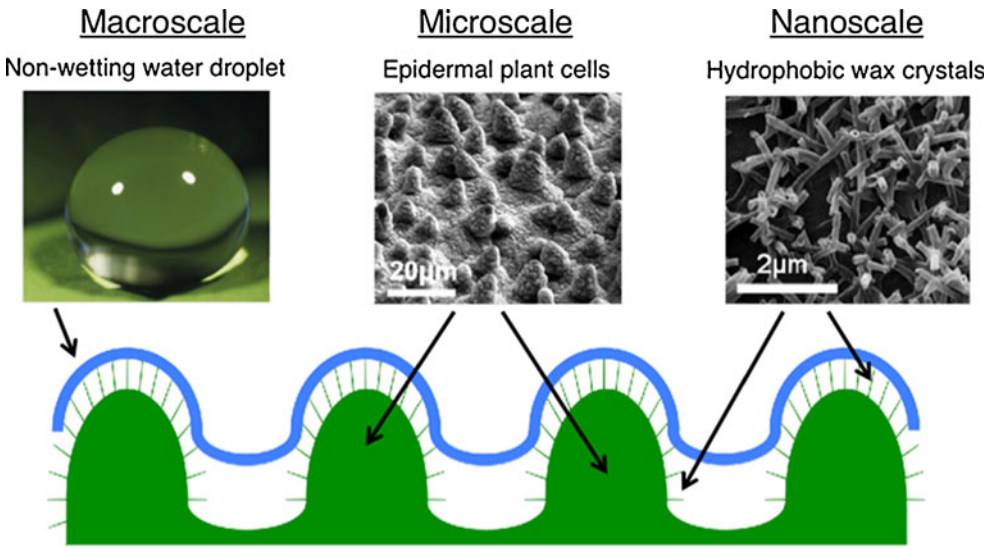

Fig. 7 The hierarchical surface structure of the lotus leaf at the micro- and nanoscale are together with the chemical properties of the hydrophobic wax crystals responsible for the macroscopic superhydrophobic phenomenon. Reprinted from Progress in Materials Science, vol. 54, Koch K. et al, Multifunctional surface structures of plants: an inspiration for biomimetics, p. 137–178, copyright (2009), with permission from Elsevier

During evaporation, a transition from Cassie–Baxter to Wenzel regime was observed. The explanation is that when the drop gets small enough, the capillary force drives the drop through the barbules and penetrates the protrusions. The measured contact angles were less than 150°, which is not strictly superhydrophobic according to the general rule. However, the hysteresis was reported to be 5–7°, making water repellence possible.

Grémillet et al. explained how the great diving bird, *Phalacrocorax carbo*, maintains body heat while obtaining food, by having a plumage that is only partly wettable, leaving an insulating layer of air between the plumage and the skin [42].

3.1.5 The Petal Effect

So far, only superhydrophobic surfaces with a low hysteresis and roll-off angle have been discussed. Studies of the petal surface of red rose (rosea Rehd) shows superhydrophobicity together with a high adhesive force with water, a remarkable effect termed the "petal effect" [43]. Water droplets are spherical in contact with the surface but do not roll off even when the petal is turned upside down. Similarly to the lotus leaf surface, the petal surface is hierarchical on the micro- and nanoscale; however, the length scales are larger. Thus, water droplets penetrate into the larger grooves, but not into the smaller ones, forming a Cassie-impregnating wetting regime [36, 44, 45]. The petal effect has also been demonstrated on *Lycopodium* surfaces [46].

3.1.6 Cuticle of Springtail (Collembola)

A very interesting group of arthropods are the surface dwelling Collembola, living on or near the soil surface. Humidity has great effect on the species composition and relative abundance in a habitat and is thus an important structural factor for their species diversity. In contrast to most terrestrial arthropods, the Collembola in general lack specific respiratory organs and therefore respire through the body surface. This makes them especially sensitive towards desiccation as the respiring part of the body surface also will allow water loss [47]. Adaptation to reduce water loss rate is crucial for the ability of Collembola to invade drier habitats and it is well documented that drought resistance reflect humidity conditions in their habitats [48]. It is quite evident that species living in drought-exposed habitat got to be robust against desiccation. However, the fact that drought-tolerant species are replaced by increasingly less tolerant species towards the wetter part of a humidity gradient suggests that there is a quite pronounced cost of adaptation to dry conditions

Several different mechanisms may be involved in Collembola drought tolerance. Some are linked to cellular processes others to the permeability of the cuticle (Fig. 8).

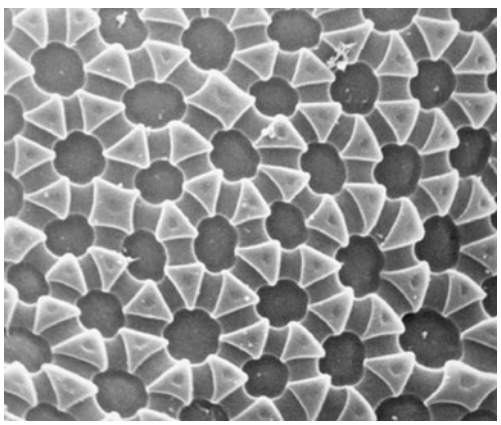

Fig. 8 The cuticle structure of Collembola. The dark circular areas consist of thin, respiring cuticle. The triangular granules with connecting lists are coated with hydrophobic wax that blocks gas exchange. Adapted with permission from [96]

In surface-dwelling species, cuticular adaptations appear to be particularly important. The collembolan cuticle has complex structures of thinner and thicker parts, and adaptation to drier habitats in many taxa involve increase in the thicker parts with wax layer preventing gas exchange at the expense of thinner respiratory parts. It is easy to imagine that a direct cost of this adaptation is reduced respiration rates. Thus, the cuticle of the Collembola represents an interesting case to examine how water loss management has been solved in nature.

In wet habitats, on the other hand, the challenge is periodical water logging and flooding. In such situations, the Collembola rely on the anti-wetting properties of the cuticle. The hydrophobic wax layer of the thicker cuticle parts is not wetted and if the thinner parts with hydrophilic surface are sufficiently small the water surface tension will prevent wetting even of the hydrophilic areas. Species with such cuticle configuration will easily float, and if submerged they will be surrounded by a film of air, similar to the water strider and the water fern (Fig. 9).

3.2 Fabrication of Biomimetic Surfaces

The biological examples discussed so far are promising sources of inspiration for the development of functional surfaces. Common for all of these examples is that they have a hierarchical surface roughness down to the nanoscale, which results in impressive functions. Therefore, to be able mimic these functions, it is necessary to be able to produce similar surface structures in a controlled manner. One of the main challenges when mimicking nature is that many natural structures can be regenerated when damaged, like the wax crystals of the lotus leaf [33]. This is however generally difficult with synthetic materials. Thus, the fabricated surface structures have to be made durable, so that they have a long lifetime before being replaced.

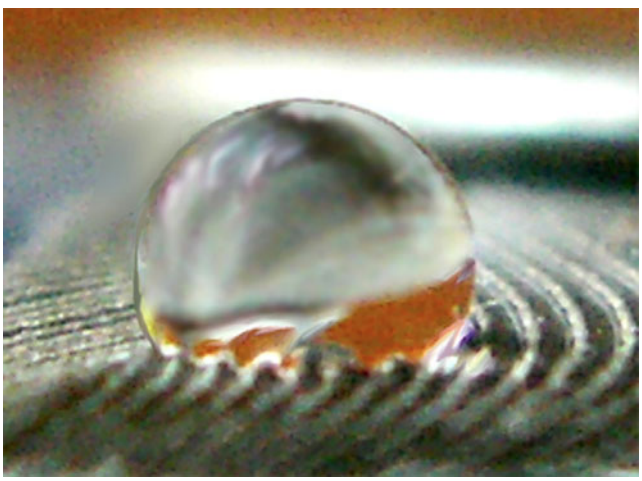

Fig. 9 A water droplet resting on the surface of a pigeon's feather, showing the high water repellence. Reprinted from Journal of Colloid and Interface Science, vol. 311, Bormashenko et al, Why do pigeon feathers repel water? Hydrophobicity of pennae, Cassie–Baxter wetting hypothesis and Cassie–Wenzel capillarity-induced wetting transition, p. 212–216, Copyright (2007), with permission from Elsevier

Fabrication of superhydrophobic surfaces is usually done by introducing surface roughness and/or changing the surface chemistry. This involves both top-down and bottom-up methods. Top-down approaches involve sculpturing of a bulk material using traditional micro-fabrication techniques such as cutting, milling, patterning and etching. In contrast, bottom-up methods use single molecules as building blocks to self-assemble or self-organise larger structural assemblies.

Both approaches have advantages and disadvantages. Top-down methods typically gives the scientist better control over the final result. However, it is generally more time-consuming and expensive compared to bottom-up methods, making mass production of nanostructured surfaces challenging. On the other hand, bottom-up methods involve a higher degree of complexity and the final result is harder to predict. Therefore, each fabrication method is often application specific.

Some materials have intrinsic hydrophobicity. This is advantageous as it simplifies the fabrication process. In this section, an overview of some fabrication methods used is presented.

3.2.1 Photolithography

Photolithography is a conventional process within microfabrication that has been used in the semiconductor industry for many years to transfer patterns on the surface of a wafer. The basic principle is to transfer a positive or negative image from a mask by exposing a photoreactive polymer with a UV-, electron- or X-ray source [49]. Due to the well-controlled reproducible results, it has mostly been used to create surfaces for examining the superhydrophobic phenomenon and the connections between surface structures and wetting behaviour [12, 18, 21, 23, 37, 50–54]. One of the earliest works by Öner et al. [18] examined the wetting quantitatively on a micro-textured surface, using photolithography and subsequent etching in silicon to produce three-dimensional pillars with various size, shapes and separations. It was found that a separation distance between the posts lower than 32 μm resulted in a non-wetting state (Cassie–Baxter) where the wetting was independent on the height of the posts. By increasing the separation distance between the posts to more than 32 μm resulted in a rapid decrease in hysteresis, a sign that the droplet transformed into the wetted Wenzel state, discussed in Section 2.

3.2.2 Replication

Replication involves creating a template that an inverted replica can be produced from. The process steps are

cheaper and faster compared to conventional photolithography for large quantity productions. Also, the method can be used with rather inexpensive polymer materials like polydimethylsiloxane (PDMS) or SU-8. The quality of the replicate depends on the spatial resolution of the template. Because reliable templates with details at the nanoscale can be fabricated, this method has a future potential in mass production of nanostructured materials.

Replicates of the surface structure of the lotus leaf have been achieved by Sun et al. [55]. Casting liquid PDMS over the leaf and subsequent curing at room temperature formed a template. Flat PDMS surfaces have a contact angle of around 100° [56]. After solidification of the template, the surface was coated with an anti-sticking monolayer. Then, liquid PDMS was poured over the template. After curing, the resulting PDMS replicate displayed a very accurate copy of the micro- and nanoscale surface of the lotus with a measured contact angle of 162°.

3.2.3 Nanoimprint Lithography

Nanoimprint lithography (NIL) is a type of replication technique. It was first demonstrated in 1995 by creating an array of holes with diameters of about 25 nm and depth of about 100 nm in a thin film of polymer resist [57]. Later, the technique has shown to be able to produce structures with a resolution down to 5 nm [58]. It uses a mechanically rigid stamp often produced by electron beam lithography [59], which is pressed down into a thin film of a soft polymer. Before the stamp is removed, the film is hardened, either by cooling or exposure of UV [59]. The resolution of the final imprint pattern is limited by the master stamp resolution and the process conditions. The advantage of NIL compared to other nanolithography techniques is that the stamps have a long lifetime. Thus, it shows potential for industrial mass production of nanostructured materials.

3.2.4 Crystal Growth

Crystallisation methods can be used to grow structural features and introduce micro- and nanoscale roughness. Crystallisation of polycrystalline copper plates to produce copper-oxide nanorods by thermal oxidation has been done by Mumm et al. [60]. After coating with a monolayer of fluorocarbons, the resulting surface exhibited a contact angle of 172°. Etching aluminium plates has also produced hierarchical surface roughness [61]. Metal surfaces can be used as templates for polymer replication.

Roughness at the nanoscale has also been achieved by growing carbon nanotubes on stainless steel substrates using chemical vapour deposition (CVD) [62–64]. CVD is a general fabrication method used in the semiconductor industry to deposit thin films of various materials, where a substrate is exposed to a reactive precursor gas. CNTs are usually grown by deposition of a metal catalyst on the substrate prior to growth, such as nickel, cobalt or iron [65]. The substrate is then heated and a process gas together with a carbon precursor gas is fed into the reaction chamber. The carbon gas reacts at the interface of the substrate and the catalyst particles to form CNTs.

Production of multi-walled CNTs on the surface of stainless steel has been achieved without any pre-deposition of catalyst, using iron-based stainless steel that acts as a catalyst by itself [62]. The fabrication of synthetic nanorods or nanowires mimics the setae of the water strider or the wax crystals of the lotus leafs. However, with these techniques, it is possible to fabricate superhydrophobic surfaces that are more durable than natural ones [66].

3.2.5 Other Methods

Phase separation (sol-gel) is an interesting method to fabricate superhydrophobic structures because it is inexpensive and easy to fabricate, where most of the process steps can be done close to room temperature. These kinds of structures can also be cut and abraded without loosing their surface roughness. Shirtcliffe et al. [67] made intrinsically superhydrophobic organosilica foams, where no need for further surface treatment was required, since the organosilica particles are hydrophobic.

Another bottom-up strategy is to assemble closely packed colloidal particles on a surface through attractive van der Waals forces between the spheres in an ordered or non-ordered structure. The magnitude of surface roughness can be tuned by choosing the particle size. Materials like silica [68] and polymer spheres [69] can be functionalized with chemical side groups to enhance hydrophobicity. This method is also inexpensive; it can be applied to large surfaces and does not require any special equipment.

Other possibilities are combinations of the aforementioned methods to produce hierarchical surface roughness, such as growth of CNTs on a surface array of colloidal particles [70] or on micro-fabricated silicon pillars [66, 71]. For further references, the excellent review of superhydrophobic fabrication methods by Roach et al. is recommended [16].

4 Applications

The examples presented so far have served as a source of inspiration for new innovative designs within various applications. With the materials and the fabrication methods available, scientists have the potential to go nature one better. However, nature's design is seldom optimised from

an engineer's point of view. It may serve other purposes under different conditions experienced by engineers. Therefore, one cannot simply copy nature blindly. A successful design must be application specific. Among the possible applications discussed here are self-cleaning, anti-icing, hydrate inhibition, anti-corrosion, drag reduction and water harvesting.

4.1 Self-Cleaning

The self-cleaning effect of the Lotus leaf is illustrated in Fig. 10. One of the first applications of superhydrophobic surfaces mimicking nature was within self-cleaning. Sto Corp. (USA) commercialised an acrylic-based exterior paint in 1999 under the registered trademark Lotusan®, named after the "Lotus-Effect". According to the company, the paint protects against particle contamination, fungal and algae growth, possess excellent weather resistance and high water vapour permeability due to the micro-texture similar to that of the lotus leaf [72].

Replacing current coating solutions with self-cleaning paints will reduce the need for cleaning chemicals. Thus, bio-inspired products may have a positive effect on the environment, as well as reducing maintenance costs. However, as the surface is exposed to the outside environment, the coating may be degraded through various ways of chemical and mechanical abrasion, such as pollution and wind. Because maintaining micro- and nano-scale roughness is essential for the self-cleaning, the effect may quickly vanish. To prevent this, the coating has to be re-applied regularly, which counteracts the purpose of making the surface permanently self-cleaning. Porous networks fabricated by sol-gel methods discussed earlier, can retain the micro-roughness even if the outermost surface is abraded. This may thus seem as an appropriate approach of producing robust functional coatings.

Fig. 10 Illustration of the self-cleaning effect exhibited by the Lotus leaf. When water droplets roll over the surface, the capillary forces acting on pollutant particles overcome the adhesive forces. Reprinted from Progress in Materials Science, vol. 54, Koch K. et al, Multifunctional surface structures of plants: An inspiration for biomimetics, p. 137–178, copyright (2009), with permission from Elsevier

Other applications where self-cleaning can be advantageous besides exterior paint, are solar panels and windows. Functional coatings for these kinds of applications need to be optically transparent. The scattering of light incident on surface increases with a larger roughness scale, reducing the transparency [16]. To avoid diffraction, surface features have to be on a length scale less than about 100 nm. Arrays of nanorods fabricated by crystal growth may seem a feasible way to go, as they are highly resistant to pressure, have extremely high specific surface areas and can be optically transparent due to their tiny dimensions [16]. Self-cleaning and anti-reflective coatings has been produced by growing ZnO nanorods using CVD, resulting in a contact angle above 160°, a hysteresis of 2° and an average reflectance in the visible range of only 2.5% [73].

4.2 Anti-Icing

Icing can lead to minor problems like reducing the visibility on the front wind shield of your car or more serious consequences like bursting pipelines due to hydrate formation, making roads slippery or cause loss of lift force on aircraft wings. Traditional methods of removing ice are mechanical scraping or through melting by heating or applying anti-freezing chemicals like salt or glycerol. However, these methods are not sustainable as they are either expensive, can cause abrasive damage to the surface or because they are toxic. Superhydrophobic coatings can have permanent anti-icing properties if the material has enough mechanical stability and resistance towards degradation. The mechanism of ice formation has been examined on hydrophilic, hydrophobic and superhydrophobic surfaces [74]. In this work, the dynamics of droplets hitting supercooled surfaces at a tilt of 30° were examined. It was observed that ice formation occurred for both hydrophilic and hydrophobic surfaces but was inhibited on the superhydrophobic surface (see Fig. 11). The reason is that impacting droplets simply bounced off the surface, minimising the heat transfer at the liquid–solid interface. Ice formation occurred at lower temperatures (−30°C). However, the ice remained in the non-wetting Cassie–Baxter state, making mechanical removal easier due to smaller contact area. In addition, it was found that closed-cell microstructures displayed the highest pressure stability against transition from Cassie–Baxter to Wenzel wetting, a property especially important in cases where droplets hit the surface at high velocities, for instance for automobile or airplane coatings.

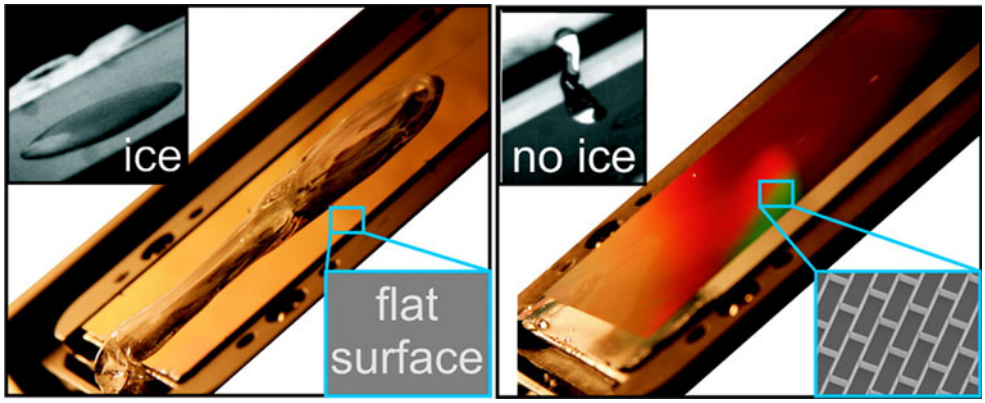

Fig. 11 Superhydrophic surfaces show ice resistance after 10 min with continuously impacting water droplets. Water droplets spreads out on the flat surface and freeze due to heat transfer. For the microstructured surface however, the droplets simply bounce off, so that ice formation is not allowed to take place. Reprinted with permission from Lidiya Mishchenko, Design of ice-free nanostructured surfaces based on repulsion of impacting water droplets, ACS Nano, 2010, 4, 7699–7707. Copyright 2010 American Chemical Society

4.3 Hydrate Inhibition

During production of natural gas, formation of hydrocarbon hydrates is an unwanted process as it tends to block pipelines. Hydrocarbon hydrates are gas molecules trapped in cage-like structures of crystalline hydrogen-bonded water molecules similar to ice. As methane gas is pumped up from deep water reservoirs at high pressures, water condenses at the pipeline sidewalls due to the low temperatures involved. The oil industry spends a large amount of resources dealing with hydrate formation each year. Common methods used are to reduce the pressure, increase the temperature or dissolve the hydrates by chemicals introduced into the pipelines. Removal of hydrates must be carefully controlled, as they dissociate into gas and water. If this process is performed too fast, it will lead to rapid gas expansion. This can cause ejection of fluid from the wells and blow outs [75].

Due to the potential problems associated with hydrate formation and the fact that none of the conventional methods are sustainable, the use of a superhydrophobic coating seems like a promising strategy. Such kind of coatings would prevent condensed water to stick to the surface and potentially prevent hydrate formation. As mentioned previously, CNTs can be grown directly on steel alloys using CVD. The carbon nanotubes provides the surface roughness at the nanoscale as well as mechanical strength, which increase the duration of the superhydrophobic coating [66]. Obviously, the greatest challenge is to coat the whole length of the pipelines, which can extend to several kilometres with minimal expenses. One strategy may be to use the natural gas, such as methane, as the precursor gas in a process step similar to that of CVD [76].

4.4 Anti-Corrosion

Fabrication of superhydrophobic surfaces on metal was discussed previously, with examples from copper, aluminium and steel. It is feasible to adopt the strategies discussed so far to fabricate metal coatings for anti-corrosion purposes. Previous work has been devoted to develop a superhydrophobic film on a copper metal surface by selective etching to produce micro- and nanostructures [77]. The surface was tested for anti-corrosion properties by immersion in seawater. After a month, no change in the contact angle was detected. The deposition of Ni-P composite coatings on carbon steel [69] also showed superhydrophobicity with corrosion-resistance. It is believed that the anti-corrosive property is because of the retention of air at the surface, so that the metal is practically kept dry even while submerged under water, mimicking the water fern.

4.5 Drag Reduction

From 1950 to 2001, the total fuel consumption in the marine industry increased worldwide by a fourfold [78]. The exhaust gases and particles released have serious impact on the marine life and must be reduced to a minimal amount. In addition, reducing the fuel consumption is of great economical interest. Due to the same reasons, reducing the air drag experienced by airplanes would be beneficial. Furthermore, drag reduction is of special interest in biosensor applications based on micro/nanofluidics, since the surface to volume ratio increases inversely with the geometric length scale [79].

Drag reduction has been exploited in the case of making coatings with riblets similar to those seen on the shark skin [80], for airplanes, ships, pipelines [81] and more recently

Table 1 Examples of hierarchical design in biological systems (adapted from [95])

Material	"Poor" constituents	Nanoscale design	Hierarchy levels
Cortical bone	Hydroxyapatite+protein	Nanocomposite	7
Nacre	Aragonite+protein	Nanocomposite	2–3
Silk	Protein	Nanocrystals	5
Crab exoskeleton	Calcite+polymer+protein	Nanocomposite	5
Sea sponge	Silica+protein	Nanocomposite	7
Diatom	Silica+protein	Nanoporous	3

swimsuits fabricated by Speedo [82]. However, all these designs have so far yielded a maximum drag reduction of only 10%.

Superhydrophobic surfaces mimicking the water fern seem a better strategy for drag reduction. Generally, it is assumed that the flow velocity is equal to zero at a solid–liquid interface (no-slip condition), and that it increases continuously with the distance normally outward from the surface [83]. However, slip at the solid–liquid interface has been identified for superhydrophobic surfaces [84]. This effect, called "giant liquid slip", is thought to be due to the air film retained at the hairy surface [29].

4.6 Water Harvesting

Finally, wetting behaviour can be utilised for collection of water in hot and arid areas. As previously discussed, the Namib Desert Beetle already accomplishes this due to the alternating hydrophobic and hydrophilic regions. A biomimetic device inspired by this design has developed by dispensing droplets of a polyacrylic acid solution [85], CF_4 plasma fluorination [86] or pulsed plasma deposition of hydrophobic polymers [87] to create an array of hydrophilic spots on a superhydrophobic surface. In the work done by Zhai et al. [85], the superhydrophobic background had a hysteresis of 3°, in contrast to the hydrophilic spots with a hysteresis of 132°. Thus, water droplets condensing on the surface rolls off the superhydrophobic surfaces and sticks to the hydrophilic regions, due to the high hysteresis. When they reach the critical size, they roll off the surface due to gravity and can subsequently be collected.

5 Discussion and Outlook

As presented in this review, there exist a number of documented methods for creating hierarchical roughness along with low surface free energy materials that leads to formation of superhydrophobic surfaces. But according to Guo et al. [88], most of biomimetic superhydrophobic surfaces cannot be applied into industry because of their weak surface mechanical properties. One example is CNT deposited directly on steel surfaces [89]. Even though they developed a successful process for growing aligned CNT on commercial steel plates they also reported that the arrays of CNT were very weakly adhered to the substrate and peeled off from the surface readily.

In order to overcome these weaknesses in mechanical properties, we propose to introduce atomistic modelling as an efficient tool in the design of nanostructured surfaces and especially focus on the insight gained from the modelling of biological materials. Biological systems typically gain their unique properties by hierarchical design (Table 1).

An example is the enhancement of mechanical properties through diatom-inspired nanoporous silica design [90, 91]. The diatoms frustules, or silicified cell walls with nanoscale size pores, are shown to be surprisingly tough when compared to bulk silica, which is one of the most brittle materials known. Through carrying out a systematic atomistic analysis, Garcia et al. captured a large variation in mechanical properties from brittle to highly ductile, where the most ductile systems with wall widths below 1 nm featured a plastic regime of almost 40%, and a

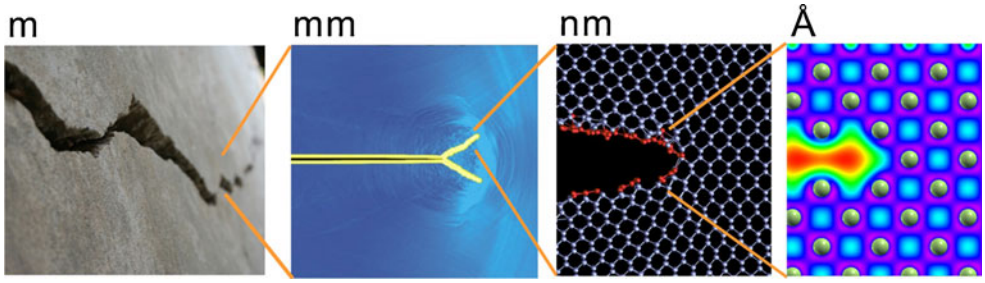

Fig. 12 Failure of materials and structures involves many length scales, from the macroscopic scale to the level of Angstrom where chemical bonds are found. A comprehensive analysis of failure must start at a fundamental level in order to represent key mechanisms of how materials fail. Adapted with permission from Macmillan Publishers Ltd: Nature [97], copyright 2010

modulus of 2.3 GPa. The most brittle responses were observed for the systems with the largest wall width, with a vanishing plastic regime, albeit a modulus of more than 30 GPa. They found that an important aspect in promoting the ductile response of the material is the ability to alter the initial rectangular shape into a hexagonal one. We intend in ongoing research to explore if it is possible to optimise both the surface properties (e.g. the relationships proposed by Zheng [23], Eq. 6) and the mechanical properties as reported above. The key tool in this research will be atomistic modelling.

Another interesting example represents the fracture of silicon. It has been known for several decades that silicon is a brittle material at low temperatures that shatters catastrophically, whereas at elevated temperatures, the behaviour of silicon changes drastically over an extremely narrow temperature range of just a few degrees and suddenly becomes ductile and soft like metals. The key to understand the transition from brittle to ductile behaviour is to consider what happens at the most fundamental level, at the tip of a crack in silicon (Fig. 12).

Recently, by using a new quantum mechanics informed model of inter-atomic interactions that is capable of examining material volumes of sufficient dimensions, new insight has been gained on the properties of silicon [92–94]. The atomistic scale investigations revealed that the emergence of very small geometric irregularities formed along the crack front is a prerequisite for the transition from brittle to ductile appearance. As the critical temperature is approached, crack tip blunting dominates and is accompanied by changes in the perfect structure at the crack tip. Bond rotations at the crack tip lead to the formation of new bond structures that differ from the hexagonal rings typically found in silicon.

The knowledge derived from the simulations reported heralds a paradigm shift in the design of conventionally brittle materials by showing that its mechanical response can be greatly altered by simple alteration of its structural geometry at the nanoscale without the need to introduce new constituents. This merger of material and structure is a powerful concept that could provide new ideas for a broader class of bioinspired materials with advanced properties. Specifically, to transform an inherently brittle material towards a very ductile one, illustrating how a weakness is turned into strength, simply by controlling its structure. This is achieved by providing large elasticity and plasticity by adding ordered nanopores to a brittle system, where the underlying mechanism change is due to surface effects and a change in the stress distribution.

To conclude, the combined optimization of both superhydrophobic nanostructured surfaces and superior bioinspired mechanical properties by atomistic modelling seems to be a promising strategy in order to introduce robust solutions of industrial use.

6 Conclusion

Structures and designs found in nature have inspired scientists to create innovative devices and materials for centuries. With the technological advances in characterization techniques, a higher level of details becomes more and more accessible. Simultaneously, a greater understanding of how molecules and particles self assemble makes it possible to design products mimicking the functional materials optimised through evolution. Lessons from nature are about discovering the connection between mechanics, structures and materials. This allows us to produce biomimetic materials with a range of possible applications. We have, in this review, discussed several biological systems, which all have remarkable surface properties. We have shown that the hierarchical arrangement of structures at the surface have a decisive impact on the macroscopic observable surface effects. Increasing the surface roughness on multiple scales by introducing nanoscale hairs or grooves superimposed on microscale asperities are necessary to increase wetting resistance and create phenomenon such as self-cleaning and water floating. By applying known fabrication methods, we can mimic those to develop functional materials with similar or better properties than nature or use the mechanisms as inspiration to improve solutions within anti-icing, anti-corrosion and hydrate inhibition among others. Main challenges include large-scale production and resistance against degradation and loss of function. As the advancement of nanotechnology continues, it is likely that sophisticated, sustainable commercial products will emerge with potential to solve some of our greatest engineering challenges in the near future. By expanding the use of atomistic modelling from hierarchical biological materials to the hierarchical surface structures discussed in this review, one may be able to find optimal designs for industrial biomimetic products.

References

1. Thompson, D. W. (1968). *On growth and form* (2nd ed.). Cambridge: Cambridge University Press.
2. Gordon, J. E. (1976). *The new science of strong materials, or why you don't fall through the floor* (2nd ed.). London: Pitman.
3. Buehler, M. J. (2010). Nanomaterials strength in numbers. *Nature Nanotechnology, 5*(3), 172–174.
4. Buehler, M. J., & Yung, Y. C. (2009). Deformation and failure of protein materials in physiologically extreme conditions and disease. *Nature Materials, 8*(3), 175–188.
5. Bhushan, B., Jung, Y. C., & Koch, K. (2009). Micro-, nano- and hierarchical structures for superhydrophobicity, self-cleaning and low adhesion. *Philosophical Transactions of the Royal Society A-Mathematical Physical and Engineering Sciences, 367*(1894), 1631–1672.
6. Buehler, M. J. (2010). Tu(r)ning weakness to strength. *Nano Today, 5*(5), 379–383.

7. Jackson, A. P., Vincent, J. F. V., & Turner, R. M. (1988). The mechanical design of nacre. *Proceedings of the Royal Society of London Series B-Biological Sciences, 234*(1277), 415–440.
8. Hiemenz, P. C., & Rajagopalan, R. (Eds.). (1997). *Principles of colloid and surface chemistry* (3rd ed.). Boca Raton, FL: CRC Press.
9. Speight, J. G., & Lange, N. A. (Eds.). (2005). *Lange's handbook of chemistry* (16th ed.). Maidenhead, UK: McGraw-Hill Professional.
10. Wenzel, R. N. (1936). Resistance of solid surfaces to wetting by water. *Industrial and Engineering Chemistry, 28*(8), 988–994.
11. Cassie, A. B. D. (1948). Contact angles. *Discussions of the Faraday Society, 3*, 11–16.
12. Patankar, N. A. (2004). Transition between superhydrophobic states on rough surfaces. *Langmuir, 20*(17), 7097–7102.
13. Nosonovsky, M., & Bhushan, B. (2005). Roughness optimization for biomimetic superhydrophobic surfaces. *Microsystem Technologies-Micro-and Nanosystems-Information Storage and Processing Systems, 11*(7), 535–549.
14. Bormashenko, E. (2010). Wetting transitions on biomimetic surfaces. *Philosophical Transactions of the Royal Society A-Mathematical Physical and Engineering Sciences, 368*(1929), 4695–4711.
15. Whyman, G., Bormashenko, E., & Stein, T. (2008). The rigorous derivation of Young, Cassie–Baxter and Wenzel equations and the analysis of the contact angle hysteresis phenomenon. *Chemical Physics Letters, 450*(4–6), 355–359.
16. Roach, P., Shirtcliffe, N. J., & Newton, M. I. (2008). Progess in superhydrophobic surface development. *Soft Matter, 4*(2), 224–240.
17. Shirtcliffe, N. J., et al. (2005). Porous materials show superhydrophobic to superhydrophilic switching. *Chemical Communications, 25*, 3135–3137.
18. Öner, D., & McCarthy, T. J. (2000). Ultrahydrophobic surfaces. Effects of topography length scales on wettability. *Langmuir, 16*(20), 7777–7782.
19. Bhushan, B., Nosonovsky, M., & Jung, Y. C. (2007). Towards optimization of patterned superhydrophobic surfaces. *Journal of the Royal Society, Interface, 4*(15), 643–648.
20. Quere, D. (2005). Non-sticking drops. *Reports on Progress in Physics, 68*(11), 2495–2532.
21. Lv, C. J., et al. (2010). Sliding of water droplets on microstructured hydrophobic surfaces. *Langmuir, 26*(11), 8704–8708.
22. Dettre, R. H., & Johnson, R. E. (1964). Contact angle hysteresis. In *Contact angle, wettability, and adhesion* (pp. 136–144). Washington DC: American Chemical Society.
23. Zheng, Q. S., et al. (2010). Small is beautiful, and dry. *Science China-Physics Mechanics & Astronomy, 53*(12), 2245–2259.
24. Amirfazli, A., & Neumann, A. W. (2004). Status of the three-phase line tension. *Advances in Colloid and Interface Science, 110*(3), 121–141.
25. Parker, A. R., & Lawrence, C. R. (2001). Water capture by a desert beetle. *Nature, 414*(6859), 33–34.
26. Gao, X. F., & Jiang, L. (2004). Water-repellent legs of water striders. *Nature, 432*(7013), 36–36.
27. Feng, X. Q., et al. (2007). Superior water repellency of water strider legs with hierarchical structures: Experiments and analysis. *Langmuir, 23*(9), 4892–4896.
28. Cernan, Z., Striffler, B. F., & Barthlott, W. (2009). Dry in the water: The superhydrophobic water fern *Salvinia*—A model for biomimetic surfaces. In S. N. Gorb (Ed.), *Functional surfaces in biology: little structures with big effects*. New York: Springer.
29. Barthlott, W., et al. (2010). The *Salvinia* paradox: Superhydrophobic surfaces with hydrophilic pins for air retention under water. *Advanced Materials, 22*(21), 2325–2328.
30. Koch, K., Bhushan, B., & Barthlott, W. (2010). Multifunctional plant surfaces and smart materials. In B. Bhushan (Ed.), *Springer Handbook of Nanotechnology* (pp. 1399–1436). New York: Springer.
31. Barthlott, W., & Neinhuis, C. (1997). Purity of the sacred lotus, or escape from contamination in biological surfaces. *Planta, 202*(1), 1–8.
32. Neinhuis, C., & Barthlott, W. (1997). Characterization and distribution of water-repellent, self-cleaning plant surfaces. *Annals of Botany, 79*(6), 667–677.
33. Koch, K., Bhushan, B., & Barthlott, W. (2009). Multifunctional surface structures of plants: An inspiration for biomimetics. *Progress in Materials Science, 54*(2), 137–178.
34. Brewer, C. A., Smith, W. K., & Vogelmann, T. C. (1991). Functional interaction between leaf trichomes, leaf wettability and the optical properties of water droplets. *Plant, Cell & Environment, 14*(9), 955–962.
35. Wagner, P., et al. (2003). Quantitative assessment to the structural basis of water repellency in natural and technical surfaces. *Journal of Experimental Botany, 54*(385), 1295–1303.
36. Marmur, A. (2004). The lotus effect: Superhydrophobicity and metastability. *Langmuir, 20*(9), 3517–3519.
37. Gao, L. C., & McCarthy, T. J. (2006). The "lotus effect" explained: Two reasons why two length scales of topography are important. *Langmuir, 22*(7), 2966–2967.
38. Zhang, L., et al. (2006). Superhydrophobic behavior of a perfluoropolyether lotus-leaf-like topography. *Langmuir, 22*(20), 8576–8580.
39. Yu, Y., Zhao, Z. H., & Zheng, Q. S. (2007). Mechanical and superhydrophobic stabilities of two-scale surfacial structure of lotus leaves. *Langmuir, 23*(15), 8212–8216.
40. Chow, T. S. (2007). Nanoscale surface roughness and particle adhesion on structured substrates. *Nanotechnology, 18*(11), 115713.
41. Bormashenko, E., et al. (2007). Why do pigeon feathers repel water? Hydrophobicity of pennae, Cassie–Baxter wetting hypothesis and Cassie–Wenzel capillarity-induced wetting transition. *Journal of Colloid and Interface Science, 311*(1), 212–216.
42. Gremillet, D., et al. (2005). Unusual feather structure allows partial plumage wettability in diving great cormorants *Phalacrocorax carbo*. *Journal of Avian Biology, 36*(1), 57–63.
43. Feng, L., et al. (2008). Petal effect: A superhydrophobic state with high adhesive force. *Langmuir, 24*(8), 4114–4119.
44. Bormashenko, E., et al. (2006). Wetting properties of the multiscaled nanostructured polymer and metallic superhydrophobic surfaces. *Langmuir, 22*(24), 9982–9985.
45. Herminghaus, S. (2000). Roughness-induced non-wetting. *Europhysics Letters, 52*(2), 165–170.
46. Bormashenko, E., et al. (2009). "Petal Effect" on surfaces based on lycopodium: High-stick surfaces demonstrating high apparent contact angles. *Journal of Physical Chemistry C, 113*(14), 5568–5572.
47. Leinaas, H. P., Slabber, S., & Chown, S. L. (2009). Effects of thermal acclimation on water loss rate and tolerance in the collembolan *Pogonognathellus flavescens*. *Physiological Entomology, 34*, 325–332.
48. Leinaas, H. P., & Hertzberg, K. (1998). Drought stress as a mortality factor in two pairs of sympatricspecies of Colembola at Spitsbergen, Svalbard. *Polar Biology, 19*, 302–306.
49. Quirk, M., & Serda, J. (2001). *Semiconductor manufacturing technology.* Columbus, OH: Prentice Hall.
50. Quéré, D. (2005). Non-sticking drops. *Reports on Progress in Physics, 68*(11), 2495–2532.
51. Wong, T. S., Huang, A. P. H., & Ho, C. M. (2009). Wetting behaviors of individual nanostructures. *Langmuir, 25*(12), 6599–6603.
52. Zheng, Q. S., Yu, Y., & Zhao, Z. H. (2005). Effects of hydraulic pressure on the stability and transition of wetting modes of superhydrophobic surfaces. *Langmuir, 21*(26), 12207–12212.
53. Yoshimitsu, Z., et al. (2002). Effects of surface structure on the hydrophobicity and sliding behavior of water droplets. *Langmuir, 18*(15), 5818–5822.

54. Nosonovsky, M. (2007). Multiscale roughness and stability of superhydrophobic biomimetic interfaces. *Langmuir, 23*(6), 3157–3161.
55. Sun, T. L., et al. (2005). Bioinspired surfaces with special wettability. *Accounts of Chemical Research, 38*(8), 644–652.
56. Bongaerts, J. H. H., Fourtouni, K., & Stokes, J. R. (2007). Soft-tribology: Lubrication in a compliant PDMS-PDMS contact. *Tribology International, 40*(10–12), 1531–1542.
57. Chou, S. Y., Krauss, P. R., & Renstrom, P. J. (1995). Imprint of sub-25 Nm vias and trenches in polymers. *Applied Physics Letters, 67*(21), 3114–3116.
58. Austin, M. D., et al. (2004). Fabrication of 5 nm linewidth and 14 nm pitch features by nanoimprint lithography. *Applied Physics Letters, 84*(26), 5299–5301.
59. Schift, H., & Kristensen, A. (2010). Nanoimprint lithography—Patterning of resists using molding. In *Springer Handbook of Nanotechnology* (pp. 273–312). New York: Springer.
60. Mumm, F., van Helvoort, A. T. J., & Sikorski, P. (2009). Easy route to superhydrophobic copper-based wire-guided droplet microfluidic systems. *ACS Nano, 3*(9), 2647–2652.
61. Lee, Y., Ju, K. Y., & Lee, J. K. (2010). Stable biomimetic superhydrophobic surfaces fabricated by polymer replication method from hierarchically structured surfaces of Al templates. *Langmuir, 26*(17), 14103–14110.
62. Baddour, C. E., et al. (2009). A simple thermal CVD method for carbon nanotube synthesis on stainless steel 304 without the addition of an external catalyst. *Carbon, 47*(1), 313–318.
63. Kim, B., et al. (2010). Synthesis of vertically-aligned carbon nanotubes on stainless steel by water-assisted chemical vapor deposition and characterization of their electrochemical properties. *Synthetic Metals, 160*(7–8), 584–587.
64. Masarapu, C., & Wei, B. Q. (2007). Direct growth of aligned multiwalled carbon nanotubes on treated stainless steel substrates. *Langmuir, 23*(17), 9046–9049.
65. Ishigami, N., et al. (2008). Crystal plane dependent growth of aligned single-walled carbon nanotubes on sapphire. *Journal of the American Chemical Society, 130*(30), 9918–9924.
66. Jung, Y. C., & Bhushan, B. (2009). Mechanically durable carbon nanotube-composite hierarchical structures with superhydrophobicity, self-cleaning, and low-drag. *ACS Nano, 3*(12), 4155–4163.
67. Shirtcliffe, N. J., et al. (2003). Intrinsically superhydrophobic organosilica sol-gel foams. *Langmuir, 19*(14), 5626–5631.
68. Tsai, P. S., Yang, Y. M., & Lee, Y. L. (2006). Fabrication of hydrophobic surfaces by coupling of Langmuir–Blodgett deposition and a self-assembled monolayer. *Langmuir, 22*(13), 5660–5665.
69. Zhu, L. Q., & Jin, Y. (2007). A novel method to fabricate water-soluble hydrophobic agent and super-hydrophobic film on pre-treated metals. *Applied Surface Science, 253*(7), 3432–3439.
70. Li, Y., et al. (2007). Superhydrophobic bionic surfaces with hierarchical microsphere/SWCNT composite arrays. *Langmuir, 23*(4), 2169–2174.
71. Chen, C. H., et al. (2007). Dropwise condensation on superhydrophobic surfaces with two-tier roughness. *Applied Physics Letters, 90*(17), 173108.
72. Sto Corp., StoCoat Lotusan. Available from: http://www.stocorp.com. Accessed on: 13 Jan 2011
73. Xiong, J., et al. (2010). Biomimetic hierarchical ZnO structure with superhydrophobic and antireflective properties. *Journal of Colloid and Interface Science, 350*(1), 344–347.
74. Mishchenko, L., et al. (2010). Design of ice-free nanostructured surfaces based on repulsion of impacting water droplets. *ACS Nano, 4*(12), 7699–7707.
75. Max, M. D. (2003). *Natural gas hydrate in oceanic and permafrost environments*. Boston, MA: Kluwer.
76. Sugimoto, S., Matsuda, Y., & Mori, H. (2009). Carbon nanotube formation directly on the surface of stainless steel materials by plasma-assisted chemical vapor deposition. *Journal of Plasma and Fusion Research, 8*, 522–525.
77. Liu, T., et al. (2007). Super-hydrophobic surfaces improve corrosion resistance of copper in seawater. *Electrochimica Acta, 52*(11), 3709–3713.
78. Eyring, V., et al. (2005). Emissions from international shipping: 1. The last 50 years. *Journal of Geophysical Research-Atmospheres, 110*(D17), D17305.
79. Bhushan, B., Wang, Y., & Maali, A. (2009). Boundary slip study on hydrophilic, hydrophobic, and superhydrophobic surfaces with dynamic atomic force microscopy. *Langmuir, 25*(14), 8117–8121.
80. Dean, B., & Bhushan, B. (2010). Shark-skin surfaces for fluid-drag reduction in turbulent flow: A review. *Philosophical Transactions of the Royal Society A-Mathematical Physical and Engineering Sciences, 368*(1929), 4775–4806.
81. Bechert, D. W., et al. (1997). Experiments on drag-reducing surfaces and their optimization with an adjustable geometry. *Journal of Fluid Mechanics, 338*, 59–87.
82. Matthews, J. N. A. (2008). Low-drag suit propels swimmers. *Physics Today, 61*(8), 32–33.
83. Batchelor, G. K. (1970). *An introduction to fluid dynamics*. Cambridge: Cambridge University Press.
84. Wang, Y. L., Bhushan, B., & Maali, A. (2009). Atomic force microscopy measurement of boundary slip on hydrophilic, hydrophobic, and superhydrophobic surfaces. *Journal of Vacuum Science & Technology A, 27*(4), 754–760.
85. Zhai, L., et al. (2006). Patterned superhydrophobic surfaces: Toward a synthetic mimic of the Namib Desert beetle. *Nano Letters, 6*(6), 1213–1217.
86. Woodward, I. S., et al. (2006). Micropatterning of plasma fluorinated super-hydrophobic surfaces. *Plasma Chemistry and Plasma Processing, 26*(5), 507–516.
87. Garrod, R. P., et al. (2007). Mimicking a stenocara beetle's back for microcondensation using plasmachemical patterned superhydrophobic-superhydrophilic surfaces. *Langmuir, 23*(2), 689–693.
88. Guo, Z., Liu, W., & Su, B.-L. (2011). Superhydrophobic surfaces: From natural to biomimetic to functional. *Journal of Colloid and Interface Science, 353*, 335–355.
89. Parthangal, P. M., Cavicchi, R. E., & Zachariah, M. R. (2007). A generic process of growing aligned carbon nanotube arrays on metal and metal alloys. *Nanotechnology, 18*, 185605.
90. Garcia, A. P., & Buehler, M. J. (2010). Bioinspired nanoporous silicon provides great toughness at great deformability. *Computational Materials Science, 48*, 303–309.
91. Garcia, A.P., D. Sen, and M.J. Buehler, *Hierarchical silica nanostructures inspired by diatom algae yield superior deformability, toughness and strength.* Metallurgical and Materials Transactions A, 2011 (in press).
92. Sen, D., et al. (2010). Atomistic study of crack-tip cleavage to dislocation emission transition in silicon single crystals. *Physical Review Letters, 104*, 235502.
93. Thaulow, C., Sen, D., & Buehler, M. J. (2011). Atomistic study of the effect of crack tip ledges on the nucleation of dislocations in silicon single crystals at elevated temperature. *Materials Science & Engineering A, 528*, 4357–4364.
94. Thaulow, C., et al. (2011). Crack tip opening displacement in atomistic modeling of fracture of silicon. *Computational Materials Science, 50*, 2621–2627.
95. Sen, D., & Buehler, M. J. (2010). Atomistically-informed mesoscale model of deformation and failure of bioinspired hierarchical silica nanocomposites. *International Journal of Applied Mechanics, 2*(4), 699.
96. Leinaas, H. P., & Fjellberg, A. (1985). Habitat structure and life-history strategies of 2 partly sympatric and closely related, lichen feeding collembolan species. *Oikos, 44*, 448–458.
97. Buehler, M. J., & Xu, Z. (2010). Mind the helical crack. *Nature, 464*(4), 42–43.